PHYSICAL REVIEW D **88,** 063002 (2013)

Parameter space metric for 3.5 post-Newtonian gravitational waves from compact binary inspirals

Drew Keppel,[1,2,*] Andrew P. Lundgren,[1,2,3,†] Benjamin J. Owen,[3,‡] and Hanyuan Zhu[3,§]

[1]*Albert-Einstein-Institut, Max-Planck-Institut für Gravitationsphysik, D-30167 Hannover, Germany*
[2]*Leibniz Universität Hannover, D-30167 Hannover, Germany*
[3]*Institute for Gravitation and the Cosmos, Department of Physics, The Pennsylvania State University, University Park, Pennsylvania 16802, USA*

(Received 25 May 2013; published 3 September 2013)

We derive the metric on the parameter space of 3.5 post-Newtonian (3.5PN) stationary phase compact binary inspiral waveforms for a single detector, neglecting spin, eccentricity, and finite-body effects. We demonstrate that this leads to better template placement than the current practice of using the 2PN metric to place 3.5PN templates: The recovered event rate is improved by about 10% at a cost of nearly doubling the number of templates. The cross correlations between mass parameters are also more accurate, which will result in better coincidence tests.

DOI: 10.1103/PhysRevD.88.063002 PACS numbers: 95.75.Pq, 95.55.Ym, 04.25.dg

I. INTRODUCTION

Many searches for gravitational waves (GWs) from coalescing compact binaries (neutron stars and/or black holes) have been conducted in data from large-scale interferometric detectors for more than a decade [1–18], and these searches will remain key science goals in the era of advanced detectors and beyond [19]. These searches achieve their sensitivity using matched filtering, which relies on the availability of template waveforms that well approximate the signals. For example, the inspiral phase of the coalescence, an adiabatic evolution of quasicircular orbits which dominates the waveform for most of the published searches, is well modeled by the post-Newtonian (PN) approximation (see [20] for a review). Here we focus on these well-modeled waveforms and mostly neglect any discrepancies with the true signals.

Even well-modeled waveforms have a parameter space to cover (for instance the masses of the compact objects) as the signal-to-noise ratio (SNR) degrades if the signal is filtered with a template with the wrong parameters, even if the latter has the correct functional form. Therefore, a key component of matched filtering searches is the construction of template banks such that, no matter where in the parameter space a signal appears, at least one template has parameters close enough to achieve a predefined fraction of the optimal SNR known as the minimal match (named in [21]; a similar concept was first mentioned in the GW literature in [22]). The match between two templates is derived from what is known in statistics as the ambiguity function (e.g., [23]), maximizing the latter over differences in extrinsic parameters to account for features of the detection algorithm such as maximization over a phase constant. Thus the match depends only on intrinsic parameters describing the shapes of the waveforms, such as masses of the two components of a binary (the distinction depends on the signal; see footnote [15] of Ref. [21]).

Construction of a template bank with a given minimal match requires an algorithm for placement of the templates in the parameter space. Ideally, one would cover the parameter space with the fewest templates given a fixed value of minimal match so as to minimize the computational cost. There are several algorithms proposed or implemented [21,24–28], involving either the construction of regular lattices in the parameter space or stochastic point selection followed by match-based selection criteria. These algorithms have varying computational costs and achieve varying approximations to the optimal (minimum) number of templates for a fixed minimal match, generally trading off those features versus robustness against parameter choices and varying dimensionality of parameter space.

All template placement algorithms can benefit at some level from the metric on the search parameter space. This metric relates the loss of match between adjacent templates to the proper distance between them in a simple and computationally cheap way as long as the proper distance is not large. For template banks with large spacing (i.e., low minimal match) such as in continuous-wave searches, the standard relation is less accurate but could be made more accurate by using the Riemannian curvature derived from the metric. The search metric has also been used in other aspects of data analysis. In particular, this metric has been used to cluster single detector triggers [29] and to check whether triggers from different detectors are coincident [30]. The search metric involves only the intrinsic parameters, and is related to but distinct from the Fisher information matrix, which has been used as a metric on the full parameter space for decades outside the field of gravitational waves—see, e.g., Ref. [23].

The two-dimensional metric for the inspiral portion of the signal associated with GWs from binary neutron stars

*drew.keppel@ligo.org
†andrew.lundgren@ligo.org
‡ben.owen@ligo.org
§hanyuan.zhu@ligo.org

(BNSs) was originally computed at 1.0 PN order [21] and then extended to 2.0 PN [31]. (The PN order refers to the highest power beyond leading order of the square of the orbital velocity kept in the waveform.) It was also noted that a different choice of coordinates resulted in a slowly varying metric that, in addition, had an analytic transformation to and from the mass coordinate space [32–34]. Recent searches for inspiral GW signals from binaries with negligible spin have used the latter form of this metric along with an optimal packing (hexagonal lattice) template placement routine in two dimensions [24]. This has been the case even when the waveforms themselves were changed to include the 3.5 PN [10] terms in the waveform phase. To enhance the sensitivity of a search at a fixed false-alarm rate (FAR), it would be better to use the metric computed to the same order as the waveforms. The reason is that there is a fitting factor issue as well as a minimal match issue: The former is a quantity similar to the latter, describing instead the loss of signal-to-noise due to imperfect waveform models [35]. Total loss of SNR is bounded above by the sum of the losses; see e.g., the discussion around Fig. 3 of Ref. [36]. Even at the same PN order there may be some remaining fitting factor issue if the templates use a different type of approximant (for example, see [37] for how different approximants of 3.5 PN order compare). We neglect this and continue to focus on parameter-space discretization issues rather than waveform modeling issues.

Hence in this work we extend the nonspinning inspiral metric of [21,31] to 3.5 PN order in phase. Preliminaries of the computation can be found in Sec. II. The metric computation itself is found in Sec. III and validations of it in Sec. IV.

II. FORMALISM

We use the stationary phase approximation (SPA) inspiral waveforms, which are known to be accurate enough for most purposes [38,39]. The general SPA inspiral waveform can be written in the form [22]

$$h(f) = \frac{\mathsf{A}(t_f)}{\sqrt{\dot{F}(t_f)}}\, \mathrm{e}^{i\Psi(t_f)} \tag{1}$$

$$= \mathcal{A}(f)\mathrm{e}^{i\Psi(f)}, \tag{2}$$

where $\mathsf{A}(t)$ is the time-domain waveform amplitude, $\dot{F}(t)$ is the instantaneous GW frequency, and t_f is defined to be the time where $F(t_f) = f$ (the Fourier frequency). The combined amplitude $\mathcal{A}(f)$ truncated at Newtonian order [22,40] is given as

$$\mathcal{A}(f) = \sqrt{\frac{5}{24}}\frac{\mathcal{M}^{-5/3}}{\pi^{2/3}D} f^{-7/6}, \tag{3}$$

where $\mathcal{M}$ is the chirp mass, which we will define later, and D is the luminosity distance to the source. For convenience, we define the frequency independent part of the amplitude to be A, where

$$A := \sqrt{\frac{5}{24}}\frac{\mathcal{M}^{-5/3}}{\pi^{2/3}D}. \tag{4}$$

The phase up to 3.5 PN order is given as [41]

$$\Psi(f) = 2\pi t_c f - \phi_c - \pi/4 + \sum_{j=0}^{7} \psi_j f^{(-5+j)/3} + \sum_{j=5}^{6} \psi_j^l \ln(f) f^{(-5+j)/3}, \tag{5}$$

where the PN coefficients $\{\psi_j, \psi_j^l\}$ are given in Appendix A in terms of the symmetric mass ratio $\eta = m_1 m_2/M^2$ and chirp mass $\mathcal{M} = M\eta^{3/5}$, where $M = m_1 + m_2$ is the total mass of the binary and m_1 and m_2 are the component masses. These intrinsic parameters affect the shape of the waveform and are fundamental to the search problem, while the extrinsic parameters (here the coalescence time t_c and coalescence phase ϕ_c) are easily searched over (see below). The combination of leading-order amplitude and higher-order phase is commonly called the restricted PN approximation [40].

In searching for well-modeled signals, such as the inspiral phase of signals associated with compact binary coalescence in a GW detector's data, the optimal filter in the sense of maximizing SNR is the matched filter. To compute the matched filter for a specific template waveform, we define the inner product between two time vectors x and y in the frequency domain as [40,42]

$$(x|y) := 4\Re \int_0^\infty \frac{\tilde{x}(f)\tilde{y}^*(f)}{S_n(f)} df, \tag{6}$$

where $\Re$ is the operator that returns the real part of its argument, $\tilde{x}(f)$ represents the Fourier transform of the vector x, * is the complex conjugate operator, and $S_n(f)$ is the single-sided power spectral density (PSD) associated with the noise of the detector. An arbitrary time delay t between the two vectors can be obtained by performing the convolution of x and y, which, according to the convolution theorem, can be written as

$$(x|y)(t) := 4\Re \int_0^\infty \frac{\tilde{x}(f)\tilde{y}^*(f)}{S_n(f)} e^{2\pi i f t} df. \tag{7}$$

In practice, the lower limit of this integral is chosen to be a point below which a negligible amount of signal power is lost, mainly a function of a detector's PSD. The upper limit depends on the frequency band for which the SPA signal has support. Ideally, matched filtering data x with a single template waveform h involves taking the inner product

$$\rho(t) = (x|h)(t). \tag{8}$$

For detection of signals with unknown time of arrival, this quantity is maximized over t (t_c in the case of inspirals), which can be done quickly and simply with a fast Fourier transform. For sinusoidal signals there is generally an

unknown constant phase offset as well (ϕ_c in the case of inspirals), which is dealt with computationally efficiently as follows: The square SNR associated with template waveform h is the sum-of-squares combination of the filter outputs of the 0 and $\pi/2$ phases of the waveform,

$$\rho^2(t) = \frac{(x|h_0)^2(t) + (x|h_{\pi/2})^2(t)}{(h_0|h_0)}. \tag{9}$$

These parameters (and others which are quickly maximized over in searches for other waveforms) are known as extrinsic parameters as opposed to intrinsic parameters affecting the waveforms shape, and the distinction affects the template placement problem as follows:

Consider the inner product between two waveforms

$$(h(\theta)|h(\theta + \Delta\theta)), \tag{10}$$

where we use $h(\theta)$ to denote a waveform with parameter vector θ^α. This is known in the statistical literature as the ambiguity function [23]. For small $\Delta\theta$ and well-behaved parameters (except for the overall amplitude), the ambiguity function falls off quadratically in $\Delta\theta$ from the maximum at $\Delta\theta = 0$,

$$(h(\theta)|h(\theta + \Delta\theta)) \approx (h(\theta)|h(\theta)) - \Gamma_{\alpha\beta}\Delta\theta^\alpha\Delta\theta^\beta, \tag{11}$$

where the Fisher information matrix,

$$\Gamma_{\alpha\beta} = (\partial_\alpha h|\partial_\beta h), \tag{12}$$

acts as a metric on the entire parameter space. (The partial derivatives are with respect to the associated parameter, i.e., $\partial_\alpha := \partial/\partial\theta^\alpha$.)

What is needed for template banks is the metric on the intrinsic parameter space. This can be obtained from a modified ambiguity function called the match in the same way that the information matrix is obtained from the ambiguity function. Let us break the vector θ^α into extrinsic parameters μ^ρ (such as the overall amplitude in general and t_c and ϕ_c for inspiral signals) and intrinsic parameters λ^μ (such as the two masses for simple inspiral signals). From here on let us also use index labels μ and ν for the intrinsic parameters only, ρ and σ for the extrinsic parameters only, and continue to use α and β for all parameters. Then we have the match as Eq. (6) normalized to unit maximum and maximized over $\Delta\mu$, and the intrinsic parameter metric as the corresponding matrix of coefficients in the expansion for small $\Delta\lambda$ [21].

The intrinsic parameter metric can also be obtained by a series of projections from the information matrix, of the form

$$g'_{\mu\nu} = g_{\mu\nu} - g^{\rho\sigma}g_{\mu\rho}g_{\nu\sigma}. \tag{13}$$

This procedure is equivalent to taking the Schur complement of the metric on the extrinsic parameter space, and is what we use below.

III. COMPUTING THE INSPIRAL METRIC

We define the moments of the detector PSD similarly to but not quite the same as other papers [21,31,34,43]. We use

$$I(q, l) := \int_{f_L}^{f_U} \frac{f^{-q/3}\ln^l(f)}{S_n(f)} df, \tag{14a}$$

$$J(q, l) := I(q, l)/I(7, 0). \tag{14b}$$

The moment functional is

$$\mathcal{J}[a] := \frac{1}{I(7,0)} \int_{f_L}^{f_U} \frac{f^{-7/3}}{S_n(f)} a(f) df, \tag{15}$$

which with our conventions yields

$$\mathcal{J}\left[\sum_q a_q f^{-q/3}\ln^l(f)\right] = \sum_q a_q J(q-7, l). \tag{16}$$

The logarithms are necessary to deal with derivatives of the higher-order PN waveforms.

We start from the normalized information matrix,

$$g_{\alpha\beta} := \frac{\Gamma_{\alpha\beta}}{\rho^2}. \tag{17}$$

Using the definition of the inner product (6), the decomposition of the waveform h (1), and the definition of the moment functional (15), the normalized information matrix takes the form

$$g_{\alpha\beta} = \mathcal{J}\left[\frac{\partial \ln \mathcal{A}}{\partial\theta^\alpha}\frac{\partial \ln \mathcal{A}}{\partial\theta^\beta}\right] + \mathcal{J}\left[\frac{\partial\Psi}{\partial\theta^\alpha}\frac{\partial\Psi}{\partial\theta^\beta}\right], \tag{18}$$

which can be expanded using (4), (5), (16), and (14) to

$$\begin{aligned} g_{\alpha\beta} = {} & \frac{\partial \ln A}{\partial\theta^\alpha}\frac{\partial \ln A}{\partial\theta^\beta}J(7,0) + (4\pi^2)\frac{\partial t_c}{\partial\theta^\alpha}\frac{\partial t_c}{\partial\theta^\beta}J(1,0) + (-2\pi)\left(\frac{\partial t_c}{\partial\theta^\alpha}\frac{\partial\phi_c}{\partial\theta^\beta} + \frac{\partial\phi_c}{\partial\theta^\alpha}\frac{\partial t_c}{\partial\theta^\beta}\right)J(4,0) \\ & + (2\pi)\sum_i\left(\frac{\partial t_c}{\partial\theta^\alpha}\frac{\partial\psi_i}{\partial\theta^\beta} + \frac{\partial\psi_i}{\partial\theta^\alpha}\frac{\partial t_c}{\partial\theta^\beta}\right)J(9-i,0) + (2\pi)\sum_i\left(\frac{\partial t_c}{\partial\theta^\alpha}\frac{\partial\psi_i^l}{\partial\theta^\beta} + \frac{\partial\psi_i^l}{\partial\theta^\alpha}\frac{\partial t_c}{\partial\theta^\beta}\right)J(9-i,1) + \frac{\partial\phi_c}{\partial\theta^\alpha}\frac{\partial\phi_c}{\partial\theta^\beta}J(7,0) \\ & + (-1)\sum_i\left(\frac{\partial\phi_c}{\partial\theta^\alpha}\frac{\partial\psi_i}{\partial\theta^\beta} + \frac{\partial\psi_i}{\partial\theta^\alpha}\frac{\partial\phi_c}{\partial\theta^\beta}\right)J(12-i,0) + (-1)\sum_i\left(\frac{\partial\phi_c}{\partial\theta^\alpha}\frac{\partial\psi_i^l}{\partial\theta^\beta} + \frac{\partial\psi_i^l}{\partial\theta^\alpha}\frac{\partial\phi_c}{\partial\theta^\beta}\right)J(12-i,1) \\ & + \sum_{i,j}\frac{\partial\psi_i}{\partial\theta^\alpha}\frac{\partial\psi_j}{\partial\theta^\beta}J(17-i-j,0) + \sum_{i,j}\left(\frac{\partial\psi_i}{\partial\theta^\alpha}\frac{\partial\psi_j^l}{\partial\theta^\beta} + \frac{\partial\psi_i^l}{\partial\theta^\alpha}\frac{\partial\psi_j}{\partial\theta^\beta}\right)J(17-i-j,1) + \sum_{i,j}\frac{\partial\psi_i^l}{\partial\theta^\alpha}\frac{\partial\psi_j^l}{\partial\theta^\beta}J(17-i-j,2), \end{aligned} \tag{19}$$

where all sums run from 0 to 7 for 3.5PN waveforms. This expansion in (18) and (19) discards the information associated with boundary terms from the derivatives. That is, derivatives of f_L and f_U are neglected. For the signals we consider, these are generally negligible since in practice f_L is generally chosen to be a constant and f_U only becomes low enough to significantly affect the moment integrals for high masses, where the search is carried out by different means.

The metric used to construct search template banks must project out the extrinsic parameters A, t_c, and ϕ_c, of which the first projection of A is trivial as the information matrix is block diagonal in that parameter [43]. This results in a two-dimensional metric on the space of intrinsic parameter only, which we refer to as the mass metric.

In the notation of [34], the mass metric $g'_{\mu\nu}$ is given as

$$g'_{\mu\nu} = \sum_{i,j,k,l} \mathbf{\Psi}_{\mu ik} \mathbf{\Psi}_{\nu jl} \Bigg[J(17-i-j, k+l) - \frac{J(12-i,k)J(12-j,l)}{J(7,0)} - \frac{[J(7,0)J(9-i,k) - J(4,0)J(12-i,k)][J(7,0)J(9-j,l) - J(4,0)J(12-j,l)]}{J(7,0)[J(1,0)J(7,0) - J(4,0)J(4,0)]} \Bigg]; \tag{20}$$

here, $\mathbf{\Psi}_{\mu i0} := \partial \psi_i / \partial \lambda^\mu$ and $\mathbf{\Psi}_{\mu i1} := \partial \psi_i^l / \partial \lambda^\mu$ make up a tensor of derivatives of PN coefficients and, for 3.5PN waveforms, the sums over i and j run from 0 to 7 and the sums over k and l run from 0 to 1.

We compute the derivatives of the phase with respect to the mass parameters $\lambda^\mu \in \{\mathcal{M}, \eta\}$. The derivatives of the PN coefficients with respect to the mass parameters can be found in Appendix B.

An alternative derivation of this metric can be obtained by using the Tanaka-Tagoshi procedure [32]. We first define a "premetric,"

$$\gamma_{\alpha\beta} = \mathcal{J}\left[\frac{\partial \Psi(f)}{\partial C^\alpha} \frac{\partial \Psi(f)}{\partial C^\beta} \right], \tag{21}$$

where $\Psi(f)$ is defined in (5) and $C^\alpha \in \{\psi_j, \psi_j^l, t_c, \phi_c\}$. These premetric components would be constant in the case where f_U is fixed. The metric of (20) is then obtained through the projection of the t_c and ϕ_c dimensions and the use of a Jacobian that transforms from the coordinates C^α to the coordinates λ^μ. We have used this as a check of our derivation.

It is in fact more desirable to plot results in terms of the so-called chirp times [44] parameters, which are similar to the C^μ. The coordinate transformation is accomplished through the use of the Jacobian,

$$g_{\mu'\nu'} = J^\mu_{\nu'} g_{\mu\nu} J^\mu_{\nu'}, \tag{22}$$

where $J^\mu_{\mu'} := \partial \lambda^\mu / \partial \lambda^{\mu'}$. The chirp times we are interested in are τ_0 and τ_3, defined as

$$\tau_0 := \frac{5}{256(\pi f_0)^{8/3} \mathcal{M}^{5/3}}, \tag{23a}$$

$$\tau_3 := \frac{\pi}{8(\pi f_0)^{5/3} \mathcal{M}^{2/3} \eta^{3/5}}, \tag{23b}$$

and are related to the phase parameters ψ_0 and ψ_3. Here f_0 is a reference frequency that, if chosen to be the lower frequency cutoff due to the noise curve, results in τ_0 being approximately the length of the Newtonian waveform and τ_3 being approximately the amount the waveform is shortened by the 1.5 PN terms. The relevant terms of the Jacobian to transform from the mass space to the chirp-times space are

$$\frac{\partial \mathcal{M}}{\partial \tau_0} = \frac{-768}{25} (\pi f_0 \mathcal{M})^{8/3}, \tag{24a}$$

$$\frac{\partial \mathcal{M}}{\partial \tau_3} = 0, \tag{24b}$$

$$\frac{\partial \eta}{\partial \tau_0} = \frac{512}{15} (\pi f_0)^{8/3} \mathcal{M}^{5/3} \eta, \tag{24c}$$

$$\frac{\partial \eta}{\partial \tau_3} = \frac{-40}{3\pi} (\pi f_0)^{5/3} \mathcal{M}^{2/3} \eta^{8/5}. \tag{24d}$$

IV. COMPARISON TO 2.0 PN METRIC

We compare the 2.0 PN and 3.5 PN versions of the two quantities most important to template placement, the square root of the determinant of the metric and the eigenvectors of the metric.

Comparing the former quantity between the different PN orders allows us to see whether the density of template banks generated using the 2.0 PN metric is sufficient. The number of templates required is given by [21,25]

$$N_{\text{templates}} = \theta(m)^{-d/2} \int \sqrt{|g'|} d^d \lambda, \tag{25}$$

where θ is a geometrical quantity associated with how the template bank tiles the parameter space, m is the maximum mismatch allowed in the template bank, d is the dimensionality of the parameter space being tiled (i.e., two for the present case as the templates are laid out in the nonspinning two dimensional chirp-time space), and $\sqrt{|g'|}$ is the square root of the absolute value of the determinant of the metric on the intrinsic parameter space.

Each template "covers" an elliptical region in intrinsic parameter space in the sense that any other waveform within that ellipse will have a mismatch with that template

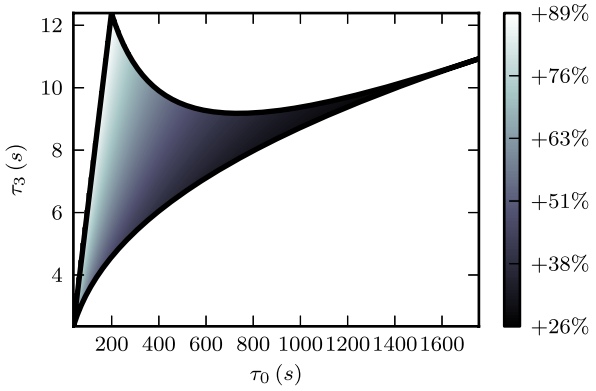

FIG. 1 (color online). Relative increase in template density $\sqrt{|g|}$ when going from the 2.0 PN mass metric to the 3.5 PN mass metric for the region of parameter space described in the text. The 3.5 PN mass metric density is between 25% and 90% larger, requiring that factor more templates to cover the same (small) region of parameter space.

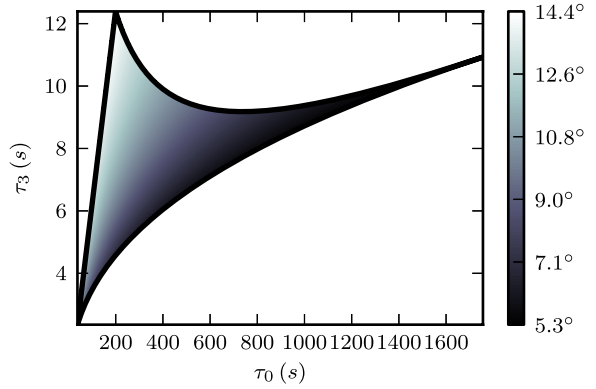

FIG. 2 (color online). Relative rotation of the eigenvectors when going from the 2.0 PN mass metric to the 3.5 PN mass metric for the region of parameter space described in the text. The largest rotations are associated with binaries with the most unequal component masses.

of no more than the (small) maximum mismatch m. (Note that we have switched from the previous notation of m for mismatch between arbitrary templates.) The elliptical shape is due to the quadratic approximation to the mismatch in (11), i.e., the approximation that all the information on the mismatch is contained in the metric rather than higher derivatives. When this approximation holds, the principal axes of the elliptical contours of constant mismatch are determined by the eigenvectors of the metric [21]. Depending on the waveform family, for mismatches of more than a few percent, the quadratic approximation degrades and the constant-mismatch contours acquire more complicated shapes than the metric ellipses.

We compare the ratio of the metric densities between the 2.0 PN metric and the 3.5 PN metric in Fig. 1 for inspiral signals associated with component masses between $1M_\odot$ and $10M_\odot$, assuming an Advanced LIGO PSD with the zero-detuning, high power configuration [45], a lower frequency cutoff of 10 Hz, and an upper frequency cutoff as the frequency associated with the inner-most stable circular orbit (ISCO) of the Schwarzschild spacetime. (The latter is the cutoff commonly used in the literature to approximate the division between the post-Newtonian inspiral and fully relativistic merger phases of coalescence.) We see that the 3.5 PN metric has a density between 25% and 90% larger than the 2.0 PN metric, with the largest effect occurring along the left-most edge of the parameter space, which corresponds to binaries with the larger mass being equal to $10M_\odot$. This effect alone implies that template banks of 3.5 PN waveforms with a minimal match of 97% laid out using the 2.0 PN metric would actually only achieve a minimal match of between ~96% and ~94%. In other words, use of the 2.0 PN template bank costs up to $0.97^3 - 0.94^3 \sim 10\%$ of the ideal detection rate.

In addition to the metric density, the eigenvectors of the metric (principal axes of the metric ellipses) also change when going from the 2.0 PN order to 3.5 PN order. For the

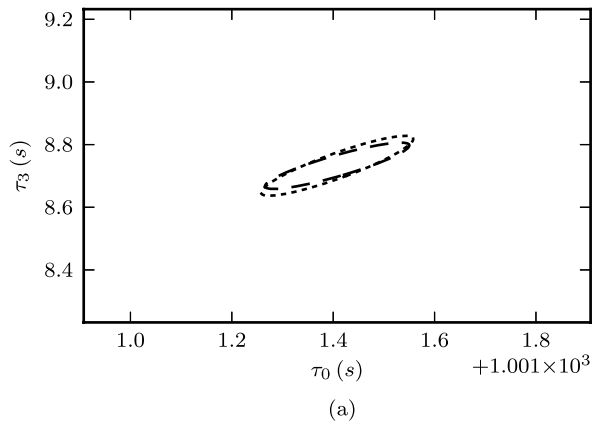

(a)

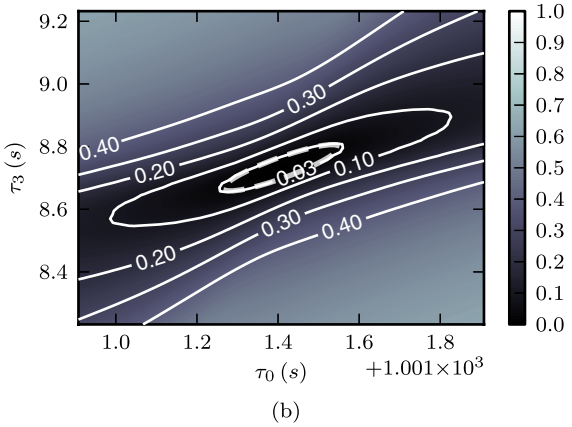

(b)

FIG. 3 (color online). (a) The 2.0 PN (dotted) and 3.5 PN (dashed) metric ellipses are compared for a BNS signal with $m_1 = m_2 = 1.4M_\odot$. (b) The 3.5 PN metric ellipse (dashed) is plotted with a size corresponding to 3% loss of SNR. The numerically computed full mismatch is shown in grey-scale with certain contours denoted by solid lines. The metric ellipse matches the 3% loss of SNR contour; for higher mismatches the contours are not elliptical.

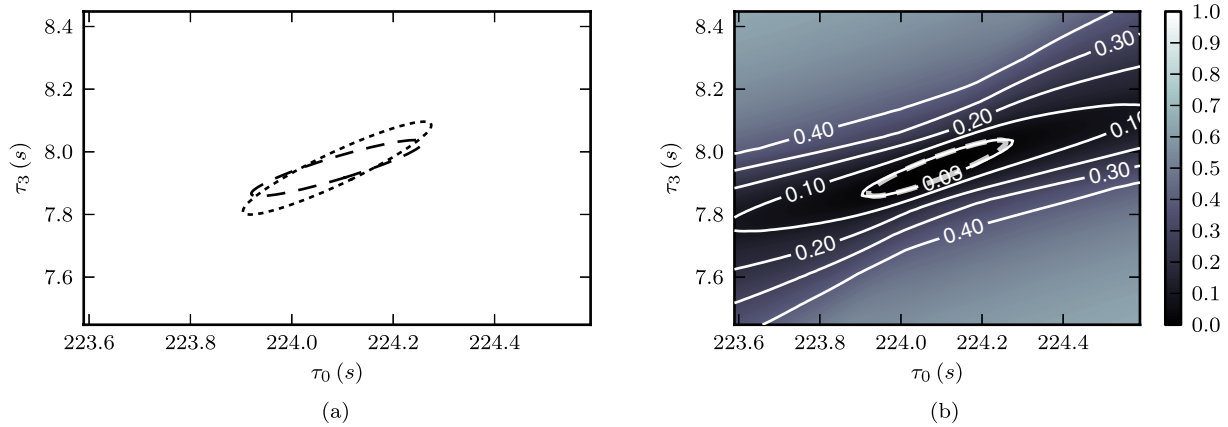

FIG. 4 (color online). (a) The 2.0 PN (dotted) and 3.5 PN (dashed) metric ellipses are compared for a neutron-star black-hole binary (NSBH) signal with $m_1 = 10M_\odot$ and $m_2 = 1.4M_\odot$. (b) The 3.5 PN metric ellipse (dashed) is plotted with a size corresponding to 3% loss of SNR. The full numerical mismatch is shown in grey scale with certain contours denoted by solid lines. The metric ellipse and the 3% loss of SNR fitting factor contour match less well than in Fig. 3(b).

same parameter space as above, this can be seen in Fig. 2. The largest rotation of the eigenvectors occurs at the upper-leftmost corner of the parameter space, which corresponds to the binaries with the most asymmetric masses (i.e., $m_1 = 3M_\odot$, $m_2 = 1M_\odot$).

These two effects are further visualized in Figs. 3(a), 4(a), and 5(a) for three points of interest in the parameter space, the points associated with BNS, neutron star/black hole (NSBH), and binary black hole (BBH), respectively, where the mass of the neutron star is a canonical $1.4M_\odot$ and the mass of the stellar mass black hole is a canonical $10M_\odot$. There we see metric ellipses associated with both the 2.0 PN and 3.5 PN mass metric. The 2.0 PN and 3.5 PN metric ellipses associated with NSBH and BBH signals disagree more than metric ellipses associated with BNS signals. This is to be expected since, for a given noise curve or frequency, waveforms of higher mass systems are more influenced by higher-order PN effects.

We also compare the 3.5 PN metric ellipses with full mismatch contours in Figs. 3(b), 4(b), and 5(b) again for points associated with BNS, NSBH, and BBH systems, respectively. Here "full" means not using the quadratic approximation but rather numerically computing the mismatch using PYLAL [46]. The BNS metric ellipse associated with 3% loss of SNR agrees well with the 3% full mismatch contour. The same is not true for the NSBH and BBH regions of parameter space. This could be because the upper frequency cutoff for signals changes as a function of the total mass of the system, which we neglect in our derivatives of the signal in (17).

Now let us look at the total number of templates. Let us use (25) with $\theta = 2/3^{3/2}$, which is exactly true for the optimal hexagonal lattice tiling of a flat two dimensional parameter space. Performing the integral in (25) numerically for the region of parameter space described above, we find that the 2.0 PN mass metric predicts that we will need

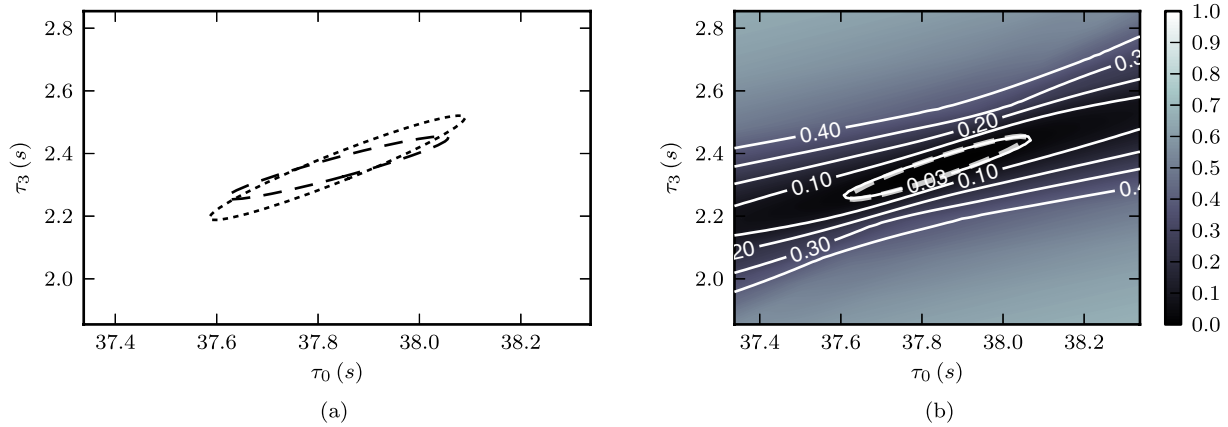

FIG. 5 (color online). (a) The 2.0 PN (dotted) and 3.5 PN (dashed) metric ellipses are compared for a binary black hole (BBH) signal with $m_1 = m_2 = 10M_\odot$. (b) The 3.5 PN metric ellipse (dashed) is plotted with a size corresponding to 3% loss of SNR. The full numerical mismatch is shown in grey-scale with certain contours denoted by solid lines. The metric ellipse and the 3% loss of SNR fitting factor contour match less well than in either Fig. 3(b) or 4(b).

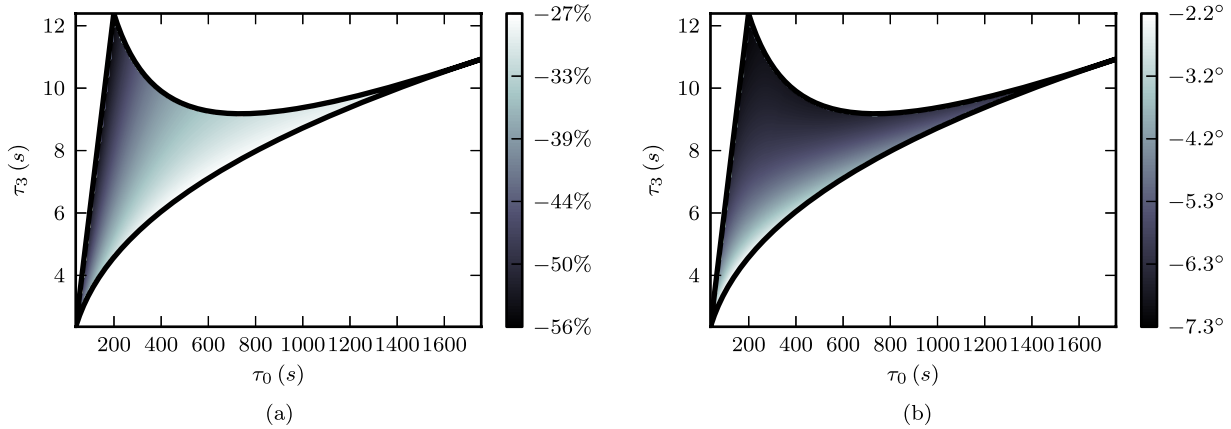

FIG. 6 (color online). (a) The fractional difference between the 3.5 PN mass metric density and the density of a 3.5 PN "fixed-mass" metric, i.e., one computed at the most mass-asymmetric point with the upper frequency cutoff set to be the Nyquist frequency, as implemented in the standard template placement algorithm [24]. The fixed-mass metric overcovers the entire parameter space. (b) The difference between the metric eigenvectors and those of the fixed mass metric. The eigenvectors of the mass metric at 3.5 PN are more aligned with those of the 3.5 PN fixed mass metric than with those of the 2.0 PN metric that varies as a function of parameter space.

1.3×10^5 templates to cover the parameter space, whereas the 3.5 PN mass metric predicts 2.0×10^5 templates. However, the hexagonal template placement algorithm utilized for previous searches [24] does not integrate the changing density. Rather it measures the metric at the most asymmetric corner of the parameter space, assumes the mass metric is invariant across parameter space, and uses the Nyquist frequency as the high frequency cutoff for the noise moments. The 3.5 PN metric density at this point is 86% larger than that of the 2.0 PN metric. If we use these point estimates in parameter space integral, this results in 1.7×10^5 and 3.2×10^5 templates for the 2.0 PN and 3.5 PN metrics, respectively. As the metric actually does vary throughout the parameter space, and as waveforms are only filtered up to the frequency associated with the ISCO, this tiling will use too many templates. This can be seen in Fig. 6 where 6(a) shows the ratio of the 3.5 PN mass metric density, which varies as a function of parameter space, to the density of the "fixed-mass" metric computed at the most asymmetric point as in [24]. Figure 6(b) shows that the orientations of the eigenvectors of the 3.5 PN metric that varies in parameter space are better aligned with those of the 3.5 PN fixed mass metric than with those of the 2.0 PN metric that varies in parameter space. Figure 7 shows the same, except replacing the 3.5 PN fixed metric with the 2.0 PN fixed metric. Although the 3.5 PN fixed metric over covers the parameter space, for constructing template banks, this is the more desirable side to err on. The orientations of the eigenvectors

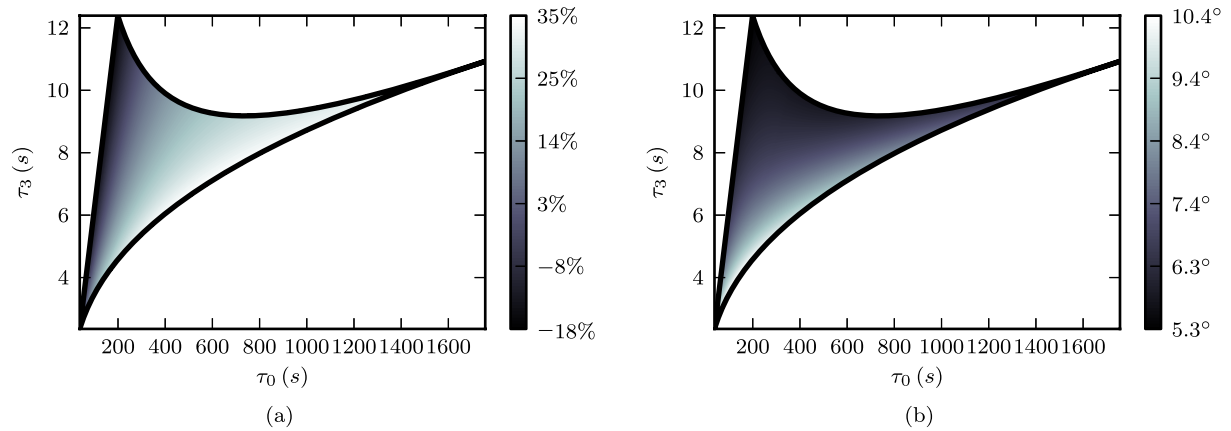

FIG. 7 (color online). (a) The fractional difference between the 3.5 PN mass metric density and the density of a 2.0 PN "fixed-mass" metric, i.e., one computed at the most mass-asymmetric point with the upper frequency cutoff set to be the Nyquist frequency, as implemented in the standard template placement algorithm [24]. The fixed-mass metric over and under covers portions of the parameter space. (b) The difference between the 3.5 PN metric eigenvectors and those of the 2.0 PN fixed mass metric. The eigenvectors of the mass metric at 3.5 PN are even less aligned with those of the 2.0 PN fixed metric than with those of the 3.5 PN fixed metric.

of the 3.5 PN fixed metric are also more aligned with the correct 3.5 PN metric than the orientations of the eigenvectors of the 2.0 PN fixed metric.

V. CONCLUSION

We have computed the inspiral metric associated with stationary phase waveforms to 3.5 PN order, extending the previously available metric at 2.0 PN order. We have shown that the metric approximates the match well for 3.5 PN waveforms for mismatch values of 3% typically used in searches. We have also characterized the error that is introduced by using a fixed metric for the entire parameter space, as in [24]. When a 2.0 PN fixed metric is used, some portions of the parameter space are under covered and some over covered compared to the target minimal match. Using a 3.5 PN fixed metric causes the entire parameter space to be overcovered, however more uniformly, a desirable feature for the template bank. Using either a fixed metric or a variable metric, the 3.5 PN template bank requires nearly twice as many templates as the equivalent 2 PN bank. Using only the change in the density of the metric, we estimate that the 3.5 PN template bank reduces the loss of ideal event rate for a typical 3%-mismatch template bank to 10% from about 20% characterizing a 2 PN template bank with 3.5 PN waveforms. The change in the parameter space metric, although it changes the number of templates, does not change the FAR for a fixed SNR threshold. This is because it is the effective independent number of templates (the waveforms that are actually used for the search) that affects the FAR, and it does so very weakly at realistic thresholds.

In addition, the 3.5 PN fixed metric more accurately reflects the orientation of the eigenvectors of the 3.5 PN metric. These results will improve coincidence test and error estimates of inspiral GW searches once the advanced detectors become operational, as they reflect a more accurate understanding of how the parameters are correlated.

ACKNOWLEDGMENTS

This work was supported by the Max Planck Gesellschaft and by National Science Foundation Grants Nos. PHY-0855589 and No. PHY-1206027. Numerical fitting factor calculations in this work were accelerated using PYCUDA [47]. This document has LIGO document No. LIGO-P1200165.

APPENDIX A: PN COEFFICIENTS

The PN coefficients ψ_i and ψ_i^l associated with the phase for different PN orders, where i is twice the PN order, are defined in terms of the symmetric mass ratio η and the chirp mass $\mathcal{M}$,

$$\psi_0 := \frac{3}{128\pi^{5/3}\mathcal{M}^{5/3}}, \tag{A1}$$

$$\psi_2 := \frac{5}{384\pi\mathcal{M}\eta^{2/5}}\left(\frac{743}{84}+11\eta\right), \tag{A2}$$

$$\psi_3 := \frac{-3\pi^{1/3}}{8\mathcal{M}^{2/3}\eta^{3/5}}, \tag{A3}$$

$$\psi_4 := \frac{5}{3072\pi^{1/3}\mathcal{M}^{1/3}\eta^{4/5}}\left(\frac{3058673}{7056}+\frac{5429}{7}\eta+617\eta^2\right), \tag{A4}$$

$$\psi_5 := \frac{5\pi}{384\eta}\left(\frac{7729}{84}-13\eta\right)[1+\ln(6^{3/2}\pi\mathcal{M}\eta^{-3/5})], \tag{A5}$$

$$\psi_5^l := \frac{5\pi}{384\eta}\left(\frac{7729}{84}-13\eta\right), \tag{A6}$$

$$\begin{aligned}\psi_6 := \frac{\pi^{1/3}\mathcal{M}^{1/3}}{128\eta^{6/5}}\Bigg(&\frac{11583231236531}{1564738560}-640\pi^2\\&-\frac{6848}{7}[\gamma+\ln(4\pi^{1/3}\mathcal{M}^{1/3}\eta^{-1/5})]\\&+\frac{5}{4}\left[\frac{-3147553127}{254016}+451\pi^2\right]\eta\\&+\frac{76055}{576}\eta^2-\frac{127825}{432}\eta^3\Bigg),\end{aligned} \tag{A7}$$

$$\psi_6^l := \frac{-107\pi^{1/3}\mathcal{M}^{1/3}}{42\eta^{6/5}}, \tag{A8}$$

$$\psi_7 := \frac{5\pi^{5/3}\mathcal{M}^{2/3}}{32256\eta^{7/5}}\left(\frac{15419335}{336}+\frac{75703}{2}\eta-14809\eta^2\right). \tag{A9}$$

Any PN coefficients of 3.5 PN or lower not defined above are identically zero. Compare Ref. [41] where these were first derived.

APPENDIX B: DERIVATIVES OF PN COEFFICIENTS

Here we give explicit expressions for the derivatives of the PN coefficients associated with the phase for different PN orders in terms of the symmetric mass ratio η and the chirp mass $\mathcal{M}$. First the derivatives with respect to $\mathcal{M}$,

$$\partial_{\mathcal{M}}\psi_0 = \frac{-5}{128\pi^{5/3}\mathcal{M}^{8/3}}, \tag{B1}$$

$$\partial_{\mathcal{M}}\psi_2 = \frac{-5}{384\pi\mathcal{M}^2\eta^{2/5}}\left(\frac{743}{84}+11\eta\right), \tag{B2}$$

$$\partial_{\mathcal{M}}\psi_3 = \frac{\pi^{1/3}}{4\mathcal{M}^{5/3}\eta^{3/5}}, \tag{B3}$$

$$\partial_{\mathcal{M}}\psi_4 = \frac{-5}{9216\pi^{1/3}\mathcal{M}^{4/3}\eta^{4/5}}\left(\frac{3058673}{7056}+\frac{5429}{7}\eta+617\eta^2\right), \tag{B4}$$

$$\partial_{\mathcal{M}}\psi_5 = \frac{5\pi}{384\mathcal{M}\eta}\left(\frac{7729}{84}-13\eta\right), \tag{B5}$$

$$\begin{aligned}\partial_{\mathcal{M}}\psi_6 = \frac{\pi^{1/3}}{384\mathcal{M}^{2/3}\eta^{6/5}}\Bigg(&\frac{10052469856691}{1564738560}-640\pi^2\\&-\frac{6848}{7}[\gamma+\ln(4\pi^{1/3}\mathcal{M}^{1/3}\eta^{-1/5})]\\&+\frac{5}{4}\left[\frac{-3147553127}{254016}+451\pi^2\right]\eta\\&+\frac{76055}{576}\eta^2-\frac{127825}{432}\eta^3\Bigg),\end{aligned} \tag{B6}$$

$$\partial_{\mathcal{M}}\psi_6^l = \frac{-107\pi^{1/3}}{126\mathcal{M}^{2/3}\eta^{6/5}}, \tag{B7}$$

$$\begin{aligned}\partial_{\mathcal{M}}\psi_7 = &\frac{5\pi^{5/3}}{48384\mathcal{M}^{1/3}\eta^{7/5}}\\&\times\left(\frac{15419335}{336}+\frac{75703}{2}\eta-14809\eta^2\right).\end{aligned} \tag{B8}$$

Now the derivatives with respect to η,

$$\partial_\eta\psi_2 = \frac{-1}{384\pi\mathcal{M}\eta^{7/5}}\left(\frac{743}{42}-33\eta\right), \tag{B9}$$

$$\partial_\eta\psi_3 = \frac{9\pi^{1/3}}{40\mathcal{M}^{2/3}\eta^{8/5}}, \tag{B10}$$

$$\begin{aligned}\partial_\eta\psi_4 = &\frac{-3}{3072\pi^{1/3}\mathcal{M}^{1/3}\eta^{9/5}}\\&\times\left(\frac{3058673}{5292}-\frac{5429}{21}\eta+1234\eta^2\right),\end{aligned} \tag{B11}$$

$$\partial_\eta\psi_5 = \frac{-\pi}{384\eta^2}\left(\frac{7729}{84}[8+5\ln(6^{3/2}\pi\mathcal{M}\eta^{-3/5})]-39\eta\right), \tag{B12}$$

$$\partial_\eta\psi_5^l = \frac{-38645\pi}{32256\eta^2}, \tag{B13}$$

$$\begin{aligned}\partial_\eta\psi_6 = \frac{-\pi^{1/3}\mathcal{M}^{1/3}}{640\eta^{11/5}}\Bigg(&\frac{11328104339891}{260789760}-3840\pi^2\\&-\frac{41088}{7}[\gamma+\ln(4\pi^{1/3}\mathcal{M}^{1/3}\eta^{-1/5})]\\&+\frac{5}{4}\left[\frac{-3147553127}{254016}+451\pi^2\right]\eta\\&-\frac{76055}{144}\eta^2+\frac{127825}{48}\eta^3\Bigg),\end{aligned} \tag{B14}$$

$$\partial_\eta\psi_6^l = \frac{107\pi^{1/3}\mathcal{M}^{1/3}}{35\eta^{11/5}}, \tag{B15}$$

$$\partial_\eta\psi_7 = \frac{-\pi^{5/3}\mathcal{M}^{2/3}}{32256\eta^{12/5}}\left(\frac{15419335}{48}+75703\eta+44427\eta^2\right). \tag{B16}$$

Any derivatives of PN coefficients of 3.5PN or lower not defined above are identically zero.

[1] H. Tagoshi *et al.* (TAMA Collaboration), Phys. Rev. D **63**, 062001 (2001).
[2] H. Takahashi *et al.* (TAMA Collaboration, LISM Collaboration), Phys. Rev. D **70**, 042003 (2004).
[3] B. Abbott *et al.* (The LIGO Scientific Collaboration), Phys. Rev. D **69**, 122001 (2004).
[4] B. Abbott *et al.* (The LIGO Scientific Collaboration), Phys. Rev. D **72**, 082001 (2005).
[5] B. Abbott *et al.* (The LIGO Scientific Collaboration), Phys. Rev. D **72**, 082002 (2005).
[6] B. Abbott *et al.* (The LIGO Scientific Collaboration), Phys. Rev. D **73**, 062001 (2006).
[7] B. Abbott *et al.* (The LIGO Scientific Collaboration and The TAMA Collaboration), Phys. Rev. D **73**, 102002 (2006).
[8] B. Abbott *et al.* (The LIGO Scientific Collaboration), Phys. Rev. D **77**, 062002 (2008).
[9] B. Abbott *et al.* (The LIGO Scientific Collaboration), Phys. Rev. D **78**, 042002 (2008).
[10] B. Abbott *et al.* (The LIGO Scientific Collaboration), Phys. Rev. D **79**, 122001 (2009).
[11] B. P. Abbott *et al.* (The LIGO Scientific Collaboration), Phys. Rev. D **80**, 047101 (2009).
[12] J. Abadie *et al.* (The LIGO Scientific Collaboration and The Virgo Collaboration), Phys. Rev. D **82**, 102001 (2010).
[13] J. Abadie *et al.* (The LIGO Scientific Collaboration and The Virgo Collaboration), Phys. Rev. D **83**, 122005 (2011).
[14] J. Abadie *et al.* (The LIGO Scientific Collaboration and The Virgo Collaboration), Phys. Rev. D **85**, 082002 (2012).
[15] J. Abadie *et al.* (The LIGO Scientific Collaboration and The Virgo Collaboration), Astrophys. J. **715**, 1453 (2010).
[16] B. Abbott *et al.* (The LIGO Scientific Collaboration), Astrophys. J. **681**, 1419 (2008).
[17] J. Abadie *et al.* (The LIGO Scientific Collaboration), Astrophys. J. **755**, 2 (2012).

[18] J. Abadie *et al.* (The LIGO Scientific Collaboration and The Virgo Collaboration), Astrophys. J. **760**, 12 (2012).
[19] G. M. Harry (LIGO Scientific Collaboration), Classical Quantum Gravity **27**, 084006 (2010).
[20] L. Blanchet, Living Rev. Relativity **9**, 4 (2006).
[21] B. J. Owen, Phys. Rev. D **53**, 6749 (1996).
[22] B. Sathyaprakash and S. Dhurandhar, Phys. Rev. D **44**, 3819 (1991).
[23] C. W. Helstrom, *Statistical Theory of Signal Detection* (Pergamon Press, London, 1968), 2nd ed..
[24] T. Cokelaer, Phys. Rev. D **76**, 102004 (2007).
[25] R. Prix, Classical Quantum Gravity **24**, S481 (2007).
[26] I. W. Harry, B. Allen, and B. S. Sathyaprakash, Phys. Rev. D **80**, 104014 (2009).
[27] C. Messenger, R. Prix, and M. A. Papa, Phys. Rev. D **79**, 104017 (2009).
[28] G. M. Manca and M. Vallisneri, Phys. Rev. D **81**, 024004 (2010).
[29] C. Robinson, B. Sathyaprakash, and A. S. Sengupta (LIGO Scientific Collaboration), Tech. Rep. No. LIGO-G070460-00-Z, 2007.
[30] C. Robinson, B. Sathyaprakash, and A. S. Sengupta, Phys. Rev. D **78**, 062002 (2008).
[31] B. J. Owen and B. Sathyaprakash, Phys. Rev. D **60**, 022002 (1999).
[32] T. Tanaka and H. Tagoshi, Phys. Rev. D **62**, 082001 (2000).
[33] R. Croce, T. Demma, V. Pierro, and I. Pinto, Phys. Rev. D **65**, 102003 (2002).
[34] S. Babak, R. Balasubramanian, D. Churches, T. Cokelaer, and B. S. Sathyaprakash, Classical Quantum Gravity **23**, 5477 (2006).
[35] T. Apostolatos, Phys. Rev. D **52**, 605 (1995).
[36] L. Lindblom, B. J. Owen, and D. A. Brown, Phys. Rev. D **78**, 124020 (2008).
[37] A. Buonanno, B. Iyer, E. Ochsner, Y. Pan, and B. Sathyaprakash, Phys. Rev. D **80**, 084043 (2009).
[38] E. Chassande-Mottin and P. Flandrin, in *Time-Frequency and Time-Scale Analysis, 1998. Proceedings of the IEEE-SP International Symposium*, p. 117.
[39] S. Droz, D. J. Knapp, E. Poisson, and B. J. Owen, Phys. Rev. D **59**, 124016 (1999).
[40] C. Cutler and E. E. Flanagan, Phys. Rev. D **49**, 2658 (1994).
[41] K. G. Arun, B. R. Iyer, B. S. Sathyaprakash, and P. A. Sundararajan, Phys. Rev. D **71**, 084008 (2005); **72**, 069903(E) (2005).
[42] L. S. Finn, Phys. Rev. D **46**, 5236 (1992).
[43] E. Poisson and C. M. Will, Phys. Rev. D **52**, 848 (1995).
[44] B. Sathyaprakash, Phys. Rev. D **50**, R7111 (1994).
[45] The LIGO Scientific Collaboration, LIGO document Report No. T0900288-v3, 2009.
[46] LIGO Scientific Collaboration, LSC Algorithm Library Suite, https://www.lsc-group.phys.uwm.edu/daswg/projects/lalsuite.html.
[47] A. Klöckner, N. Pinto, Y. Lee, B. Catanzaro, P. Ivanov, and A. Fasih, Parallel Comput. **38**, 157 (2012).